Aqueous Humour Dynamics in the Anterior Chamber and Its Influence on Acute Angle-Closure Glaucoma

Zuhaila Ismail
Department of Mathematical Sciences, Faculty of Science, Universiti Teknologi Malaysia

Han Nee Yong
Department of Mathematical Sciences, Faculty of Science, Universiti Teknologi Malaysia

Yeou Jiann Lim
Department of Mathematical Sciences, Faculty of Science, Universiti Teknologi Malaysia

Maimunah Abdul Muna' aim
Ophthalmology Unit, Faculty of Medicine and Health Sciences, Universiti Sains Islam Malaysia

https://doi.org/10.5109/7395666

出版情報：Proceedings of International Exchange and Innovation Conference on Engineering & Sciences (IEICES). 11, pp.1219-1224, 2025-10-30. International Exchange and Innovation Conference on Engineering & Sciences
バージョン：

Aqueous Humour Dynamics in the Anterior Chamber and Its Influence on Acute Angle-Closure Glaucoma

Zuhaila Ismail[1], Han Nee Yong[1], Yeou Jiann Lim[1] and Maimunah Abdul Muna'aim[2]
[1]Department of Mathematical Sciences, Faculty of Science, Universiti Teknologi Malaysia, 81310 UTM Johor Bahru, Johor, Malaysia.
[2]Ophthalmology Unit, Faculty of Medicine and Health Sciences, Universiti Sains Islam Malaysia, Nilai, Negeri Sembilan 71800, Malaysia.
Corresponding author email: zuhaila@utm.my

Abstract: *Acute angle closure glaucoma (AACG) is a critical ophthalmic condition characterized by a sudden rise in intraocular pressure (IOP) due to impaired AH flow within the anterior chamber (AC) of the human eye. This study presents a mathematical model to investigate AH dynamics under normal and pathological conditions associated with angle narrowing and pupillary block. The model couples the incompressible Navier-Stokes and heat equations, incorporating physiologically realistic boundary conditions such as fluid secretion and drainage through the porosity of the trabecular meshwork. Three simplified geometric representations of the AC are employed: a healthy eye, angle-narrowing eye, and one exhibiting pupillary block. Simulations are conducted using COMSOL Multiphysics to analyse velocity fields, IOP, and temperature effects. Results reveal that anatomical changes and flow resistance contribute to elevated IOP. The findings enhance understanding of AACG mechanisms and offer quantitative insight for guiding clinical risk assessment and treatment planning of AACG.*

Keywords: Mathematical model; Aqueous humour; Anterior chamber; AACG; Human eye;

1. INTRODUCTION

The human eye preserves its physiological and structural integrity through highly regulated mechanisms that govern intraocular fluid dynamics. The anterior chamber, located between the cornea and the iris, is occupied by aqueous humour (AH), a transparent Newtonian fluid that plays a fundamental role in maintaining intraocular pressure (IOP) and supplying essential nutrients to avascular structures such as the cornea and crystalline lens [1]. The production, transport, and drainage of AH are tightly coordinated to support ocular homeostasis. AH is actively secreted by the non-pigmented epithelial cells of the ciliary body, passes through the posterior chamber, flows across the pupil into the anterior chamber, and is primarily drained through the conventional outflow pathway, which includes the trabecular meshwork and Schlemm's canal. A smaller proportion of AH exits the eye via the uveoscleral pathway, representing the unconventional drainage route [2].

Disruptions in this physiological circulation – whether associated with age-related anatomical changes or predisposing ocular conditions – can compromise the delicate balance of IOP regulation, leading to pathological elevations. Such imbalance is a key factor in the pathogenesis of acute angle-closure glaucoma (AACG), a vision-threatening ophthalmic emergency characterised by a sudden and marked rise in IOP due to obstruction of aqueous outflow through the anterior chamber angle [3, 4]. According to Quigley [5], among glaucoma subtypes, AACG is especially concerning due to its abrupt onset and the potential for irreversible optic nerve damage and permanent vision loss within hours if not treated promptly.

Anatomical predispositions play a central role in the development of AACG. The incidence of AACG rises significantly with age, often triggered by lens-related changes. Ageing contributes to progressive lens thickening and anterior displacement, which narrows the anterior chamber angle and increase the risk of angle closure [6]. Individuals with hyperopic eyes, short axial lengths, or shallow anterior chambers are particularly susceptible, as their anatomical configuration facilitates mechanical obstruction of the trabecular meshwork and precipitating an acute glaucomatous crises [7]. The sudden occlusion of the trabecular meshwork by the peripheral iris prevents the AH outflow, leading to a rapid increase in IOP [8].

Flores-Sanchez and Tatham [9] mentioned that the most common initiating mechanism in AACG is pupillary block, where resistance to AH flow from the posterior to anterior chambers causes a pressure gradient that bows the iris forward – a phenomenon known as iris bombé – leading to sudden angle closure. Other non-pupillary block mechanisms include plateau iris configuration, where the ciliary body pushes the peripheral iris forward and phacomorphic glaucoma, due to swollen or intumescent lens [10]. Additionally, angle crowding may arise from a shallow anterior chamber, anteriorly positioned lens, or short axial length, all of which reduce the space available for aqueous outflow and exacerbate angle closure risk [11]. These factors reduce available space for AH drainage at the trabecular meshwork, thus increasing the risk of angle closure.

From a fluid dynamics perspective, AH flow is governed by a combination of pressure gradients and thermal convection [12]. The slight temperature differences between the corneal surface and internal ocular structures induce buoyancy-driven circulation within the anterior chamber [13]. In a healthy eye, AH flow maintains a stable pattern that facilitates nutrient transport and waste removal. However, when the drainage angle becomes compromised – as in AACG – the increased resistance at the outflow site impedes fluid movement and leads to elevated IOP. Even small structural variations in the

trabecular meshwork or iris configuration can significantly disrupt these delicate flow dynamics [14].

Mathematical modelling offers a powerful framework to understand and predict intraocular fluid dynamics under pathological conditions. Previous computational studies have focused on steady-state or chronic scenarios of open-angle glaucoma, employing Navier-Stokes to simulate flow within simplified eye geometries. For instance, [15] utilized a lattice Boltzmann model to simulate aqueous humour dynamics, incorporating incompressible Navier-Stokes flow, heat convection and diffusion, and Darcy seepage flow. Similarly, [16] presented a comprehensive computational model to simulate the coupled dynamics of aqueous humour flow and heat transfer in the human eye, accounting for convective effects due to temperature variations. However, fewer models capture the transient, nonlinear flow behaviour and geometric deformation associated with AACG onset. Modelling such phenomena is inherently challenging due to dynamic configuration of ocular tissues, and the complex interactions between the iris, lens, and cornea.

This study aims to develop a computational model of AH flow during AACG, integrating anatomical realism with physiologically relevant boundary conditions. Specifically, it investigates the effects of pupillary block, angle narrowing, and corneal-iris proximity on IOP, velocity fields, and temperature distribution within the anterior chamber. The model simulates geometries that represent varying degrees of angle closure and introduces two main control parameters: the rate of AH inflow at the ciliary body and the resistance-driven outflow at the trabecular meshwork. These parameters are critical for replicating the pathophysiological conditions characteristic of AACG. Numerical simulations are performed using the finite element method implemented in COMSOL Multiphysics, enabling the coupling of fluid dynamics with thermal transport. This modelling approach provides a novel framework for understanding how alterations in fluid input and drainage interact with anatomical constriction to trigger pathological pressure spikes. By elucidating the fluid mechanical consequence of angle closure, this work seeks to advance the quantitative understanding of AACG progression and support the development of diagnostic and therapeutic strategies.

2. MATHEMATICAL FORMULATION

In this study, two-dimensional models of the anterior segment of the human eye are developed under three anatomical conditions: (i) a normal eye, (ii) an eye with angle narrowing, and (iii) an eye exhibiting pupillary block. The fluid domain includes the posterior chamber, pupil aperture, anterior chamber, and trabecular meshwork as illustrated in Figure 1.

The AH is treated as an incompressible Newtonian fluid with constant viscosity and density, In the anterior and posterior chamber, the flow is governed by the steady-state incompressible Navier Stokes equations [17] as demonstrated in Eq. (1-3). The thermal convection is included to model temperature-driven buoyancy effects within the AH. The steady-state heat transport equation [18] is given by

$$\frac{\partial u}{\partial x}+\frac{\partial v}{\partial y}=0. \tag{1}$$

$$\rho\left(u\frac{\partial u}{\partial x}+v\frac{\partial u}{\partial y}\right)+\frac{\partial p}{\partial x}-\mu\left(\frac{\partial^2 u}{\partial x^2}+\frac{\partial^2 u}{\partial y^2}\right)+\rho g\alpha(T-T_c)=0. \tag{2}$$

$$\rho\left(u\frac{\partial v}{\partial x}+v\frac{\partial v}{\partial y}\right)+\frac{\partial p}{\partial y}-\mu\left(\frac{\partial^2 v}{\partial x^2}+\frac{\partial^2 v}{\partial y^2}\right)=0. \tag{3}$$

$$k\left(\frac{\partial^2 T}{\partial x^2}+\frac{\partial^2 T}{\partial y^2}\right)-\rho c\left(u\frac{\partial T}{\partial x}+v\frac{\partial T}{\partial y}\right)=0. \tag{4}$$

where u and v indicate the velocity of AH in the x and y direction respectively, p represents the pressure of AH, and T refers to the temperature of AH. Gravitational acceleration, g=9.8ms^{-1} , acts in the positive x-direction under normal condition. All other variables in Eq. (1-4) describing the fluid properties of AH and thermal properties are obtained from [19, 20] as illustrated in Table 1.

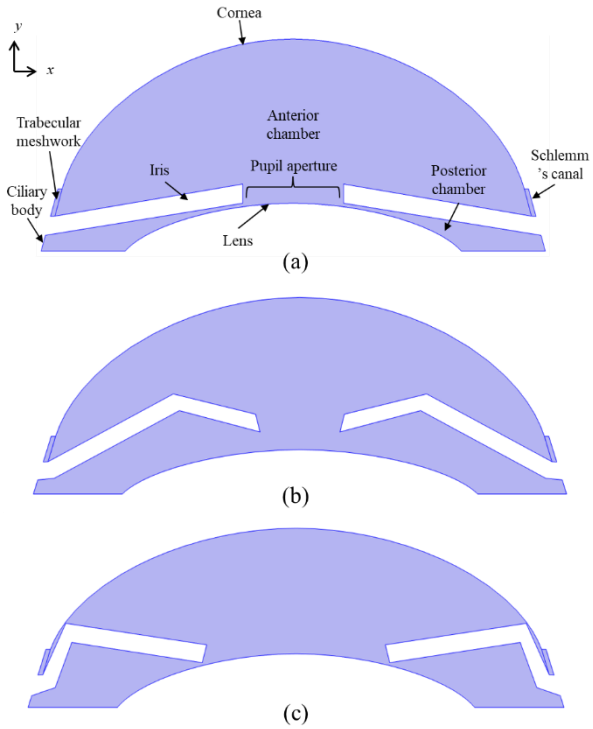

Fig. 1. Geometry of model for (a) normal eye, (b) eye with angle narrowing, and (c) eye with pupillary block.

Table 1. Values of fluid and thermal properties.

Description	Value
Thermal expansion coefficient of AH, α	3.37×10^{-4}K^{-1}
Specific heat, c	3997 Jkg^{-1}K^{-1}
Thermal conductivity, k	0.58Wm^{-1}K^{-1}
Dynamic viscosity, μ	0.74×10^{-3}kgm^{-3}
Density, ρ	996kgm^{-3}
Temperature at inner eye, T_p	310.15K
Temperature at cornea surface, T_c	308.15K
Porosity of trabecular meshwork, ε	0.15
Permeability of trabecular meshwork, κ	2×10^{-15}m^2

In the trabecular meshwork, the flow is modelled using the Stokes-Brinkman equations [21] to account for the porous resistance while preserving continuity with the adjacent fluid domain in Eq. (5).

$$\nabla p = -\frac{\mu}{\kappa}\boldsymbol{u} + \frac{\mu}{\varepsilon}\nabla^2\boldsymbol{u} \quad (5)$$

where κ denotes the permeability tensor of trabecular meshwork while ε represents the porosity of trabecular meshwork with values as shown in Table 1.

The model applies physiologically relevant boundary conditions to replicate the flow environment during AACG as illustrated in Figure 2. A fixed uniform velocity is prescribed at the inlet, $v_0 = 2 \times 10^{-6}$ ms^{-1}, corresponding to the normal rate of AH production at the ciliary body [22]. A pressure boundary condition is applied at the Schlemm's canal, representing the normal outflow resistance where pressure in the normal eye is set at $p_0 = 13.5$ mmHg while pressure in the pathologic eye is fixed at $p_0 = 27$ mmHg [23]. At all other walls, no-slip boundary condition, $\boldsymbol{u} = 0$, is applied. A fixed temperature, T_c, is imposed at the corneal surface and a higher temperature, T_p, is applied at other internal eye surfaces.

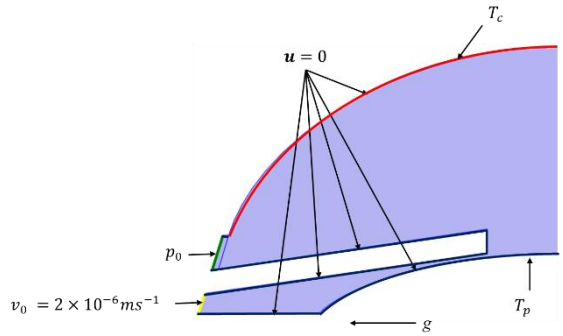

Fig. 2. Boundary conditions of the model.

2.1 Computational Mesh and Validation

A numerical simulation is carried out using COMSOL Multiphysics, employing the finite element method for solving the coupled fluid and heat equations. To ensure mesh-independent result, a grid refinement study is performed using the normal eye model. Four different mesh densities are tested and the simulated results are shown in Table 3.

Table 3. Mesh test result for different mesh density

Mesh	Element size	Domain element	Maximum velocity
1	Normal	4434	4.7685E-4
2	Fine	6746	4.7679E-4
3	Finer	16984	4.7690E-4
4	Extra fine	43046	4.7690E-4

The maximum velocity magnitude within the anterior chamber is monitored as indicators of convergence. As illustrated in Table 3, results stabilized beyond the finer mesh. Therefore, the finer mesh configuration (Mesh 3) is adopted for all simulations to ensure both accuracy and computational efficiency.

To validate the model and numerical implementation, the predicted velocity field under normal anatomical conditions is compared against published data. Although the geometric models are slightly different, an excellent qualitative agreement is observed in Figure 3.

Notably, the maximum velocity magnitude in the anterior chamber is used as a benchmark parameter as it is sensitive to both anatomical structure and inflow-outflow boundary conditions. The current model predicts a maximum anterior chamber velocity of 4.7695×10^{-3} ms^{-1}. Under equivalent parameters and assumptions, there is a slight contrast in the velocity magnitude with the numerical findings of Chen et al. [24]. Nevertheless, the difference is minor and thus, this value is considered consistent and in agreement with the previously validated study.

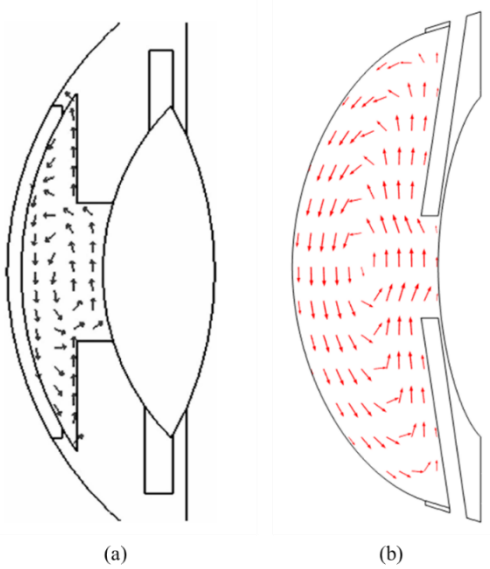

Fig. 3. Comparison of AH streamlines between (a) Shafahi and Vafai [25] and (b) present study.

3. RESULTS AND DISCUSSION

In the normal eye model (see Figure 4(a)), a characteristic circulating flow loop is observed, driven by a combination of pressure gradients and buoyancy forces due to temperature difference between the cornea and internal ocular structures. AH first flows from the posterior chamber through the pupil into the anterior chamber, travels along the posterior cornea, and drains through the trabecular meshwork. The maximum velocity magnitude occurs near the corneal surface – consistent with previously reported results [26, 27].

In the angle-narrowing model (see Figure 4(b)), a significant alteration in the flow pattern is observed. As the iridocorneal angle becomes restricted, resistance to outflow increases, particularly in the inferior angle where drainage is compromised. This leads to a localized build-up of velocity and pressure near the narrowed region. The circulation loop becomes distorted, with slower return flow in the inferior chamber, indicating reduced clearance of AH.

In the pupillary block model (see Figure 4(c)), a sharp reduction in aqueous flow from the posterior to the anterior chamber is observed, with AH accumulating in the posterior chamber. This results in iris bowing forward (iris bombé), further occluding the trabecular meshwork. The velocity within the anterior chamber is significantly reduced, while elevated flow speeds are confined to a thin jet-like region around the periphery of the pupil, where partial fluid escape occurs.

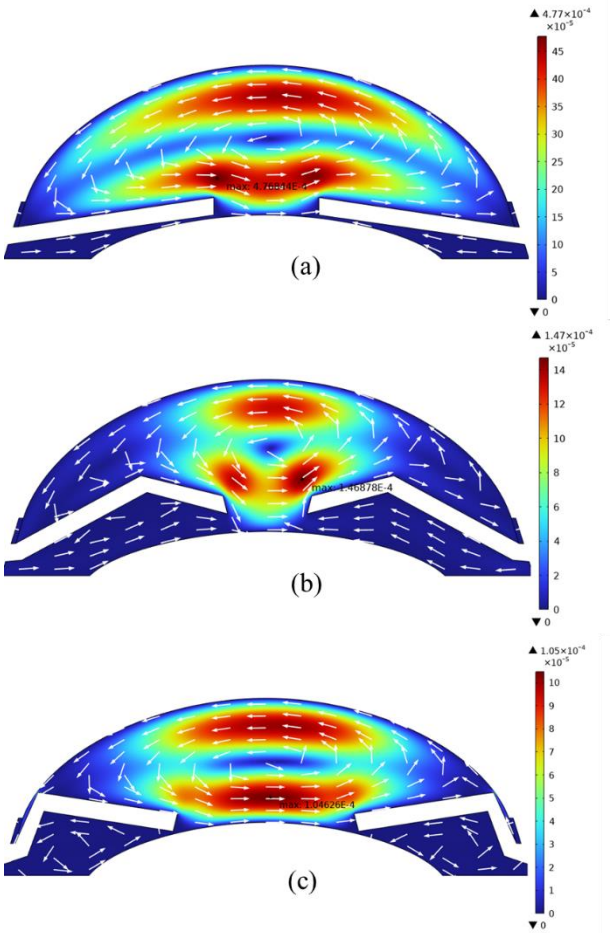

Fig. 4. Velocity distribution in (a) normal eye, (b) eye with angle-narrowing, and (c) eye with pupillary block.

IOP is evaluated across all three anterior chamber models under varying physiological and pathological conditions. The analysis is divided into two primary investigations: the impact of different AH inflow velocities at the ciliary body and the effect of outlet resistance modulated via the porosity and permeability of the trabecular meshwork.

In order to investigate the influence of AH production on IOP, simulations are conducted under four inflow velocities. The inflow velocity, $v_0 = 2{\times}10^{-6}$ ms^{-1}, at the ciliary body is used as a baseline. Two cases are studied: the normal eye with permeability, $\kappa = 7 \times 10^{-15}$ and porosity, $\varepsilon = 0.22$, while the pathologic eye with permeability, $\kappa = 2.3 \times 10^{-15}$ and porosity, $\varepsilon = 0.16$ [28]. The corresponding IOP in the anterior chamber for each eye model is shown in Table 4. Across all inflow velocities, the normal eye maintains a stable and physiologically acceptable IOP level at approximately 1900 Pa (14 mmHg), consistent with healthy AH dynamics [9].

However, the angle-narrowing and pupillary block models exhibit significant IOP elevation, with the angle-narrowing configuration consistently producing higher pressure levels than pupillary block eye. Although both are well above the clinical threshold for healthy eyes, the angle-narrowing eye exhibits the highest IOP increase, indicating that even moderate anatomical obstruction significantly reduces the efficiency of aqueous drainage. The pupillary block model, even though more severe anatomically, exhibits a slightly lower IOP than the angle-narrowing model across all inflow conditions. This is likely due to localized accumulation in the posterior chamber not being fully captured by anterior chamber pressure. These elevated pressures suggest the onset of AACG in both pathological cases as IOP in AACG cases typically exceeds 30 mmHg (approximately 5333 Pa) [9]. Among the two, the angle-narrowing eye demonstrates more severe impairment, likely due to widespread peripheral resistance and geometric obstruction at the drainage angle.

Table 4. IOP of different eye under varying inlet velocities

Velocity ms^{-1}	Normal eye (Pa)	Angle - narrowing eye (Pa)	Pupillary block eye (Pa)
$v_0/2$	1866.5	3695.2	3678.0
v_0	1874.6	3732.1	3697.8
$1.5v_0$	1882.7	3769.0	3717.5
$2v_0$	1890.9	3806.0	3737.3

A second parametric study explored the influence of structural resistance of trabecular meshwork, characterized by porosity and permeability, on IOP. Table 5 summarizes the simulated IOP values under varying permeability profiles. The IOP of normal eye, although elevated, remains below AACG diagnostics. In comparison, the angle-narrowing and pupillary block models both exceeds 3800 Pa (approximately 28.5 mmHg), indicating severe outflow obstruction and high risk of glaucomatous damage.

These results confirm that AH drainage resistance is a dominant factor in pathophysiology of AACG, particularly when compounded with unfavourable anatomy. Notably, while the pupillary block model shows elevated pressure, it is the angle-narrowing model that reaches the highest IOP under both scenarios – suggesting that gradual, widespread narrowing of the angle may lead to more severe, insidious pressure elevation compared to localized pupillary block. The simulation reinforces the importance of monitoring anatomical predispositions and outflow facility as early diagnostic markers.

Table 5. IOP of different eye under varying porosity and permeability values

ε	κ (m^2)	Normal eye (Pa)	Angle - narrowing eye (Pa)	Pupillary block eye (Pa)
0.4	7.59E-14	1859.9	3660.5	3659.5
0.3	2.35E-14	1863.2	3665.5	3662.2
0.2	5.33E-15	1879.7	3690.1	3675.4
0.1	5.27E-16	2073.8	3980.6	3830.4

Temperature contours demonstrate that the corneal cooling effect drives convection in the anterior chamber. In all models, a thermal gradient is established between the cooler cornea and warmer internal eye structures, promoting a negative x flow along the corneal surface and positive x flow along the iris.

In the normal model (see Figure 5(a)), the thermal circulation is symmetric and contributes to the overall stability of AH motion. In the angle-narrowing model (see Figure 5(b)), the thermal loop becomes asymmetric, with delayed cooling in the inferior region. In the pupillary block model, thermal circulation is largely disrupted (see Figure 5(c)), with temperature becoming more stratified, particularly in the posterior chamber,

where fluid stagnation almost occurs. These observations suggest that thermal effects, while secondary to pressure-driven flow under normal conditions, becomes more pronounced in pathological states, potentially compounding stagnation and affecting flow dynamics.

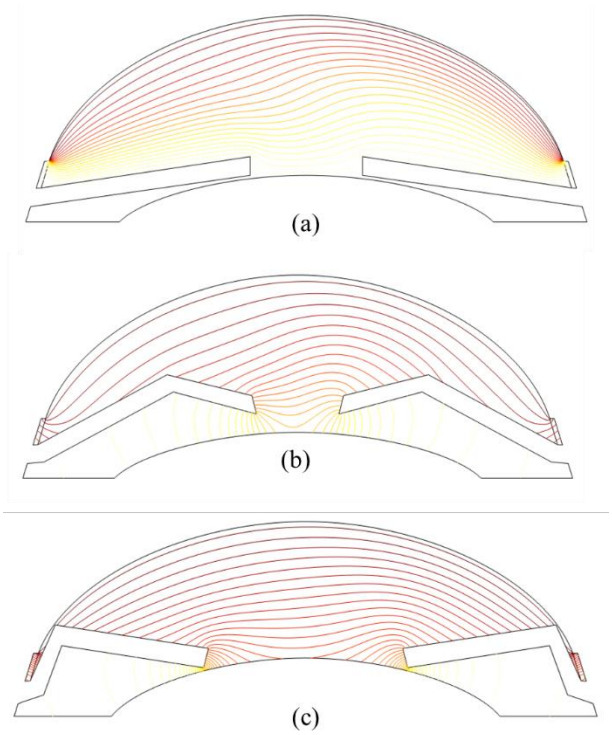

Fig. 5. Temperature contours in (a) normal eye, (b) eye with angle-narrowing, and (c) eye with pupillary block.

The results of this study illustrate the complex interplay between anatomical geometry, fluid resistance, and thermal convection in the pathophysiology of AACG. In early stages of angle narrowing, altered circulation may precede noticeable IOP changes, indicating a potential early diagnostic marker. The pupillary block model demonstrates how blockage of posterior-to-anterior flow leads to rapid pressure escalation, reinforcing the clinical urgency associated with this condition. Moreover, the coupled modelling approach shows that both thermal and mechanical effects must be considered when simulating intraocular flow. The inclusion of realistic geometry and physiological processes allows for a more accurate representation of AH dynamics in diseased states.

4. CONCLUSION

This study presents a computational investigation of AH flow in the anterior chamber of the eye under conditions simulating AACG. Three geometrical models – a healthy eye, an eye with angle narrowing, and an eye exhibiting pupillary block – are developed to assess the impact of anatomical constriction on flow behaviour and IOP. The finite element simulations, performed using COMSOL Multiphysics, couple the Navier-Stokes equations with heat equation to account for both fluid flow and thermal convection. The results show that

(a) Both increased inflow velocity and decreased outflow permeability contribute significantly to IOP elevation.

(b) Angle narrowing can lead to more severe pressure elevations than pupillary block, particularly under conditions of elevated inflow or impaired drainage.

These findings provide quantitative insights into how anatomical predispositions and fluid dynamic alterations synergize to induce pathological pressure spikes. The model offers a robust framework for simulating different glaucomatous scenarios and supports future integration with patient-specific geometries and diagnostic imaging data such as CT-imaging [29]. Future extensions of this model could include time-dependent simulations to capture acute onset dynamics, fluid-structure interaction to model iris deformation during iris bombé, or advanced hybrid solvers such as Lattice Boltzmann-FEM coupling [30].

ACKNOWLEDGEMENT

This research was funded by the Universiti Teknologi Malaysia (UTM), UTM Fundamental Research Vote No: Q.J130000.3854.23H02 and Q.J130000.3854.23H57.

REFERENCES

[1] Goel, M., R.G. Picciani, R.K. Lee, et al., Aqueous humor dynamics: a review, The Open Ophthalmology Journal, 4 (2010) 52-59.
[2] Mark, H.H., Aqueous humor dynamics and the iris, Med Hypotheses, 60 (2003) 305-8.
[3] Foster, P.J., R. Buhrmann, H.A. Quigley, et al., The definition and classification of glaucoma in prevalence surveys, Br J Ophthalmol, 86 (2002) 238-42.
[4] Weinreb, R.N., T. Aung, and F.A. Medeiros, The pathophysiology and treatment of glaucoma: a review, JAMA, 311 (2014) 1901-11.
[5] Quigley, H.A., Glaucoma, The Lancet, 377 (2011) 1367-1377.
[6] He, M., P.J. Foster, G.J. Johnson, et al., Angle-closure glaucoma in East Asian and European people. Different diseases?, Eye, 20 (2006) 3-12.
[7] Ritch, R., M.B. Shields, and T. Krupin, *The glaucomas*. 2nd ed ed. 1996: Mosby.
[8] Maria Fea, A. and L. Bertaina, Angle Closure Glaucoma: Pathogenesis and Evaluation. A Review, Journal of Clinical & Experimental Ophthalmology, 01 (2012)
[9] Flores-Sanchez, B.C. and A.J. Tatham, Acute angle closure glaucoma, Br J Hosp Med (Lond), 80 (2019) C174-C179.
[10] Tabatabaei, S.M., G. Fakhraie, S. Ansari, et al., Plateau Iris: A Review, J Curr Ophthalmol, 35 (2023) 11-16.
[11] Yang, M.C. and K.Y. Lin, Drug-induced Acute Angle-closure Glaucoma: A Review, J Curr Glaucoma Pract, 13 (2019) 104-109.
[12] Bhandari, A., Ocular Fluid Mechanics and Drug Delivery: A Review of Mathematical and Computational Models, Pharm Res, 38 (2021) 2003-2033.
[13] Бутенко, Л.Л., Н.В. Пасєчнікова, В.О. Науменко, et al., Heat exchange in the human eye: a review, Oftalmologicheskii Zhurnal, (2022) 50-58.
[14] Carreon, T., E. van der Merwe, R.L. Fellman, et al., Aqueous outflow - A continuum from trabecular

meshwork to episcleral veins, Prog Retin Eye Res, 57 (2017) 108-133.
[15] Qin, Z., L. Meng, F. Yang, et al., Aqueous humor dynamics in human eye: A lattice Boltzmann study, Math Biosci Eng, 18 (2021) 5006-5028.
[16] Saigre, T., V. Chabannes, C. Prud'Homme, et al., Mathematical modeling and simulation of coupled aqueous humor flow and temperature distribution in a realistic 3D human eye geometry, arXiv preprint arXiv:2502.09119, (2025)
[17] Heys, J.J. and V.H. Barocas, A boussinesq model of natural convection in the human eye and the formation of Krukenberg's spindle, Ann Biomed Eng, 30 (2002) 392-401.
[18] Ooi, E.H. and E.Y. Ng, Simulation of aqueous humor hydrodynamics in human eye heat transfer, Comput Biol Med, 38 (2008) 252-62.
[19] Karampatzakis, A. and T. Samaras, Numerical model of heat transfer in the human eye with consideration of fluid dynamics of the aqueous humour, Phys Med Biol, 55 (2010) 5653-65.
[20] Bhandari, A., A. Bansal, and N. Sinha, Effect of aging on heat transfer, fluid flow and drug transport in anterior human eye: A computational study, J Control Release, 328 (2020) 286-303.
[21] Loke, C.Y., E.H. Ooi, M.S. Salahudeen, et al., Segmental aqueous humour outflow and eye orientation have strong influence on ocular drug delivery, Applied Mathematical Modelling, 57 (2018) 474-491.
[22] Jen, W.W., Z. Ismail, and A. Fitt, Simulation of Aqueous Humour Flow Driven by Buoyancy Effects and Flow Through Pupil Aperture During Descemet Membrane Detachment, CFD Letters, 12 (2020) 12-23.
[23] Wang, W., X. Qian, H. Song, et al., Fluid and structure coupling analysis of the interaction between aqueous humor and iris, BioMedical Engineering OnLine, 15 (2016)
[24] Chen, H., F. Zhang, Y. Huang, et al., Numerical investigation of topical drug transport in the anterior human eye, International Journal of Heat and Mass Transfer, 85 (2015) 356-366.
[25] Shafahi, M. and K. Vafai, Human Eye Response to Thermal Disturbances, Journal of Heat Transfer, 133 (2011)
[26] Ooi, E.H. and E.Y.K. Ng, Effects of natural convection within the anterior chamber on the ocular heat transfer, International Journal for Numerical Methods in Biomedical Engineering, 27 (2010) 408-423.
[27] Chen, P., Y. Zhu, and K. Yao, Descemet membrane detachment in femtosecond laser-assisted cataract surgery: a case report, BMC Ophthalmol, 17 (2017) 169.
[28] Ferreira, J.A., P. de Oliveira, P.M. da Silva, et al., Numerical simulation of aqueous humor flow: From healthy to pathologic situations, Applied Mathematics and Computation, 226 (2014) 777-792.
[29] Zaw Linn, H. and M. Todo, Computational Study on Femoral Fracture using CT-Image based Finite Element Method, Proceedings of International Exchange and Innovation Conference on Engineering & Sciences (IEICES), 7 (2021) 58-63.
[30] Sawayama, K., T. Tsuji, and Y. Fujimitsu, Coupling Approach of Lattice Boltzmann Fluid Simulation and Finite Element Analysis of Geophysical Properties: Application to Natural Rock Fracture in Geothermal Area, Proceedings of International Exchange and Innovation Conference on Engineering & Sciences (IEICES), 5 (2019) 73-76.